CORA Cork Open Research Archive
Cartlann Taighde Oscailte Chorcaí

Title	Characterization and functional properties of pH- and heated time-induced aggregates from red lentil protein
Authors	Du, Han;Lin, Yichen;Stanton, Catherine;Daniloski, Davor;Zannini, Emanuele;Ross, R. Paul;Miao, Song
Publication date	2023-07-28
Original Citation	Du, H., Lin, Y., Stanton, C., Daniloski, D., Zannini, E., Ross, R.P. and Miao, S. (2023) 'Characterization and functional properties of pH- and heated time-induced aggregates from red lentil protein', Food Structure, 37, 100342 (12 pp). https://doi.org/10.1016/j.foostr.2023.100342.
Type of publication	Article (peer-reviewed)
Link to publisher's version	10.1016/j.foostr.2023.100342
Rights	© 2023 Published by Elsevier Ltd. © This manuscript version is made available under the CC-BY-NC-ND 4.0 license https://creativecommons.org/licenses/by-nc-nd/4.0/ - https://creativecommons.org/licenses/by-nc-nd/4.0/
Download date	2026-11-17 11:35:04
Item downloaded from	https://hdl.handle.net/10468/15284

UCC
University College Cork, Ireland
Coláiste na hOllscoile Corcaigh

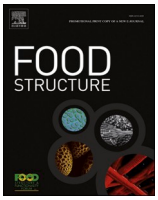
Food Structure 37 (2023) 100342



Contents lists available at ScienceDirect

Food Structure

journal homepage: www.elsevier.com/locate/foostr





Characterization and functional properties of pH- and heated time-induced aggregates from red lentil protein

Han Du [a,b], Yichen Lin [a,b], Catherine Stanton [a,d], Davor Daniloski [a,e], Emanuele Zannini [b], R. Paul Ross [d], Song Miao [a,c,*]

[a] Teagasc Food Research Centre, Moorepark, Fermoy, Co., Cork, Ireland
[b] School of Food and Nutritional Sciences, University College Cork, Cork, Ireland
[c] China-Ireland International Cooperation Centre for Food Material Sciences and Structure Design, Fujian Agriculture and Forestry University, Fuzhou 350002, China
[d] APC Microbiome Ireland, University College Cork, Cork, Ireland
[e] Victoria University, Advanced Food Systems Research Unit, Institute for Sustainable Industries and Liveable Cities and College of Health and Biomedicine, Melbourne, VIC 8001, Australia

ARTICLE INFO

Keywords:
Plant protein
Fibrillar
Particulate
Aggregation
Structure

ABSTRACT

In this study, red lentil isolate protein (RLPI, 3 %, w/v) was treated at pH 2 and 7 at 85 °C for a period of 0–24 h. The TEM and SDS-PAGE results indicated that the molecular weight of RLPI was steadily reduced and hydrolyzed into peptides over the prolonged heating time, eventually forming fibrillar and particulate aggregates at pH 2 and 7, respectively. The FTIR results showed an increased level of the proteins' random coil motifs due to the excessive heating. According to the results of emulsifying properties, the emulsifying capabilities of fibrillar proteins were higher than those of the particle proteins at the same protein concentration due to the proteins' structure and their surface charge. Notably, the fibrillar aggregates formed a gel network structure and stronger interactions in fibrillar aggregates compared to the particulate aggregates at pH 2. This study provides references for the processing and utilization of plant proteins in beverages and dietary supplements.

1. Introduction

With the rapid growth of population, the production of animal protein and the maintenance of environmental ecology are under enormous pressure. There is an increasing interest in the food industry into replacing the animal proteins with alternative protein sources that are high in nutritional value (Joehnke et al., 2021). Plant proteins from a variety of sources, such as legumes, cereals, and oil seeds, have been identified as possible alternatives due to their adaptability, high protein content, low cost, and favorable nutritional profile (Ladjal-Ettoumi et al., 2015; Ren et al., 2021; Tan et al., 2021). Lentil (*lens culinaris*) is a highly nutritious legume with an abundant quantity of carbohydrates. It is rich in proteins (20.6 %−31.4 %), fibers, vitamins, and minerals, and low in fat and cholesterol (Gunes & Can Karaca, 2021; Yadav et al., 2007). Lentil protein is composed of approximately 70 % globulin, 16 % albumin, 11 % gluten, and 3 % prolamin. Globulins contain both legumin (11S) and vicilin (7S)-like proteins (Barbana & Boye, 2011). In general, lentil proteins are extracted by alkaline extraction/isoelectric precipitation, and their molecular weight ranges from 18 to 100 kDa (Lee et al., 2021).

Food protein fibrils are increasingly being employed in emulsion and foam systems, hydrogels, nutrient transporters, and other applications. However, a vast number of protein fibril research studies have been concentrated on animal proteins (Hu et al., 2019; Wei & Huang, 2020; Zhang et al., 2020). Namely, after a few hours of thermal treatment at 85 °C, whey protein could generate amyloid-like fibrils at pH 2.0 (Cui et al., 2022). The protein molecules aggregate thus forming long fibrils due to the hydrophobic interaction between non-polar regions on the surface of the denatured proteins. On the contrary, the formation of amyloid-like fibrils was obtained from purified phaseolin, rich kidney protein isolate (7 S globulin), at 85 ℃ and at pH 2.0. Particularly, by using transmission electron microscopy (TEM), atomic force microscopy (AFM), and spectroscopic techniques the study found that the morphology of the formed fibrils was closely dependent upon the heating time, and the heating resulted in remarkable conformational changes of the protein, as well as polypeptide hydrolysis (Tang et al., 2010).

To strengthen the use of plant proteins in the food industry, it is

* Corresponding author at: Teagasc Food Research Centre, Moorepark, Fermoy, Co., Cork, Ireland.
E-mail address: song.miao@teagasc.ie (S. Miao).

https://doi.org/10.1016/j.foostr.2023.100342
Received 19 March 2023; Received in revised form 19 July 2023; Accepted 25 July 2023
Available online 28 July 2023
2213-3291/© 2023 Published by Elsevier Ltd.

important to comprehend the formation mechanism and characteristics of plant protein aggregates as well as their functional properties. The size and structure of aggregates formed when protein solutions were heated at different pH levels have been reported to be determined by the heating protocol, protein concentration, pH, and the presence or absence of salt (van der Linden & Venema, 2007). The isoelectric point (pI) of protein extracted from red lentil is 4.5 by the isoelectric precipitation technique (Alonso-Miravalles, et al., 2019). As globular proteins are thermally treated, their structure partially unfolds, resulting in protein aggregation. Depending on the morphology of the aggregates, they can be classified as spherical particles (near to the pI of the protein), flexible strands (pH = 7), and semi-flexible fibrils (pH < 2.5 and low ionic strength) (Amagliani & Schmitt, 2017). To our best knowledge, Li et al. (2021) compared the structural characterisation of cowpea, chickpea, and lentil protein fibrils. The particle size decreased and then expanded when the heat time increased, allegedly due to restructuring of the ordered structure of the proteins after proteolytic hydrolysis. In particular, after the thermal treatment, legumin oligomers would dissociate and reorganize via hydrophobic contacts and sulfhydryl/disulfide bond exchange processes, resulting mostly in high-molecular-weight aggregates (Mession et al., 2015). For pea protein isolate, in the presence of 7 S globulins, steric hindrance and electrostatic repulsions would minimize the aggregation of legumin predominantly via non-covalent bonds (Mession et al., 2015). Furthermore, it has been shown a strong correlation between concentration and aggregation rate when soy protein isolate was heated in aqueous solution at neutral pH (Chen et al., 2016). The pH of the plant protein solution not only affects the protein solubility but also its structural unfolding during denaturation. According to Lee et al. (2021), lentil protein exhibits different physicochemical as a function of pH. Although, a few studies have investigated the mechanisms of a plant protein to form different types of aggregates and investigated the structural and functional changes that take place during this process (Lee et al., 2021; Li et al., 2021), limited focus was allocated to observe the importance of the red lentil's effect on the structure and functionality of its protein.

Therefore, the purpose of the current research was to examine the characteristics of various types of aggregate derived from red lentil protein isolate (RLPI). Different aggregate degree samples were evaluated for their microstructure, secondary structure, proteins' charge, emulsifying characteristics, and gelation behavior. The correlation between the types of aggregates and functional properties was discussed. The findings will assist in understanding the conformational changes of RLPI under certain environmental conditions that might give some indication regarding their behaviour during food processing and subsequently their utilization when manufacturing novel plant-based products.

2. Materials and methods

2.1. Materials

The RLPI (85.13 % protein, w/w) was separated using the isoelectric precipitation technique and was gifted by the Food and Nutritional Sciences Department, University College Cork, Cork, Ireland. The sample powder was created by isolating the aqueous protein, extracting it by acid precipitation at pH 4.5, neutralised with 3 M NaOH, pasteurized for 30 min at 65 ℃, and spray dried (T_{in}: 180 ℃, T_{out}: 75 ℃) (Alonso--Miravalles et al., 2019). Thermo Fisher Scientific Inc. (Waltham, USA) supplied the Thioflavin T (ThT). Moreover, 12 % precast polyacrylamide gel, 10–250 kDa protein maker methanol, glacial acetic acid, and Coomassie brilliant blue R250 were purchased from Bio-Rad Laboratories Inc. (Hercules, USA); 1-Anilino-8-naphthalene-sulfonate (ANS), sodium chloride (NaCl) and the other chemical reagents were purchased from Sigma (St. Louis Mo, USA). The solutions were prepared with Milli-Q water. Finally, the pH of all solutions was measured with a calibrated pH meter equipped with a combined pH electrode, temperature sensor, and fixed cable (Metrohm AG, Oberdorfatrasse, Herisau, Switzerland).

2.2. Preparation of red lentil protein aggregates

The RLPI (3 %, w/v) was dissolved in deionized water containing 150 mM NaCl stirred for 4 h, and then the solutions were adjusted at pH values of 2 and 7, using either 1 M HCl or NaOH, respectively. After hydrating the protein solutions overnight at room temperature, the samples were centrifuged at 10,000 g for 20 min and filtered to remove insoluble material. According to the solubility of red lentil protein in different pH (Fig. S1), the protein concentrations of the samples were 1.78 % (w/v) at pH 2 % and 1.79 % (w/v) at pH 7. All experiments were conducted at this concentration unless otherwise specified. A water bath was used to aggregate the protein solutions at 85 °C (0, 1, 2, 4, 6, 12, 18, 24 h). When the samples were heated, they were immediately chilled in an ice bath to a refrigerator temperature. The samples were stored at 4 ℃ for analyses within three days, and aliquots of the samples were frozen and freeze-dried at − 50 ℃ for 48 h (Beta 1–8 LSC plus freeze-dryer/Martin Christ Gefriertrocknungsanlagen GmbH, Osterode am Harz, Germany) to obtain powders for the FTIR measurements.

2.3. Thioflavin T (ThT) fluorescence spectroscopy

The process of RLPI aggregation at pH 2 and 7 over time was determined by measuring the ThT fluorescence intensity following the Nilsson (2004)'s approach with slight adjustments. The stock solution was prepared by mixing the powder of ThT with phosphate buffer (10 mM, pH 7.0) containing 150 mM NaCl. The stock solution was filtered through a 0.22 μm filter and kept at 4 °C in the dark. Working solution was prepared by dilution the stock solution by 50 times with the same buffer. After mixing for at least one minute, 100 μL sample was added to 3 mL ThT working solution. Fluorescence spectrophotometer (Agilent Technologies Germany GmbH & Co. KG/ Waldbronn, Germany) measurements were made at 440 nm (excitation) and 490 nm (emission) for the mixtures. Working solution fluorescence intensity was subtracted as a background signal by setting the slits at 10 nm.

2.4. Transmission electron microscopy (TEM)

Microstructures of the RPLI (0.02 %, w/v) were observed using a JEOL TEM (2100 F, Japan) operating at 200 kV in a bright field imaging mode. The samples were prepared by placing a droplet of dispersion on a commercial TEM grid (copper lacey carbon grid, 300 mesh, SPI supplies); after a minute of deposition, the excess of the sample was removed.

2.5. Sodium dodecyl sulfate-polyacrylamide gel electrophoresis (SDS-PAGE)

The protein profiles of the samples were determined according to the method of Laemmli (1970) by using SDS-PAGE (12 % precast gel). Three times diluted samples were mixed with a loading buffer (3−1), and heated for 10 min at 85 ℃. The protein marker and sample solution were loaded into each well and run at a constant voltage of 100 V. Methanol/glacial acetic acid/water (1:1:3) solutions were used to destain the gel after it had been stained with Coomassie brilliant blue R250.

2.6. Zeta (ζ)-potential and particle size analysis

Measurements were performed using the Zetasizer Nano ZS (Malvern Instrument Ltd., Worcestershire, UK) to determine ζ-potential and particle size. In order to measure the ζ- potential, the sample solutions were diluted 300 times stepwise. The instrument was equilibrated for 60 s, and three measurements were taken for each sample. Particle size measurements were conducted with diluted samples in the same manner

as the ζ-potential to 600 times. A 1.5 mL sample of the diluted solution was then placed in cuvettes. The equilibration time was 120 s, and three measurements were conducted for each sample (Karaca et al., 2011). Regarding the data obtained, each sample was independent and the peaks were classified according to the proportion.

2.7. Intensity fluorescence

The sample solutions were diluted 30 times stepwise. Fluorescence spectra (λ_{ex}, 280 nm, λ_{em}, 290–420 nm, slit width = 5 nm) were measured with a fluorescence spectrophotometer at 600 nm/min.

2.8. Surface hydrophobicity (H_0)

Surface hydrophobicity of the RLPI in the solutions was measured using a fluorometric assay method with 1-anilinonaphthalene-8-sulfonic acid (ANS; Sigma Aldrich, St Louis, MO, USA) as a fluorescence probe. The relative fluorescence intensity (RFI) was measured at excitation and emission wavelengths of 390 and 470 nm, respectively, using a Shimadzu fluorescence spectrophotometer (5301-PC, Shimadzu Corp., Kyoto, Japan) following the method of Li et al. (2019) with slight modifications. The sample solutions were 3–30 times diluted. The H_0 was determined by plotting fluorescence intensity against protein concentration to obtain the initial slope.

2.9. Fourier transform infrared spectroscopy (FTIR)

Fourier transform infrared (FTIR) spectroscopy (Bruker Tensor 27, Bruker Optik GmbH, Germany) was used to determine the secondary structures of proteins using previously prepared freeze-dried samples at pH 2 and 7 (see Section 2.2). Powder samples were covered in sample cells, and infrared absorption spectra were collected at wavelengths between 400 and 4000 cm^{-1}. Each spectrum consisted of an average of 100 scans with a resolution of 4 cm^{-1}. The OPUS 7.5 software (Bruker Optik GmbH, Germany) was used for the atmospheric corrections (H_2O and CO_2 compensations). Origin software was used to fit Gaussian band profiles to the Amide I band region (1700–1600 cm^{-1}) (Curley et al., 1998). The research of Daniloski, McCarthy, Auldist, et al. (2022) was used as a reference to assign the absorption bands (Table 3 and Table 4).

2.10. Emulsifying activity index (EAI) and emulsifying stability index (ESI)

Both, EAI and ESI of the samples were determined following the method of Shevkani et al. (2015) with a slight modification. The protein solutions (1.78 % and 1.79 % [w/v] for pH 2 and pH 7, respectively [see Section 2.2]) were diluted 3 times. Subsequently, 18 mL of protein solution was mixed with 2 mL of sunflower oil at 18,000 rpm for 1 min with an Ultra-Turrax (IKA-25, Staufen, Germany). A 30 μL of the emulsion from the bottom of the tube was gently pipetted and stirred with 2970 μL of 1 % (w/v) SDS at 0 and 10 min. The resulting absorbance was read at 500 nm employing a spectrophotometer. According to Pearce and Kinsella (1978), the EAI and ESI are calculated using the following formulae:

$$\mathrm{EAI}\ (m^2/g) = \frac{2 \times 2.303 \times A_0 \times DF}{C \times \varphi \times \theta \times 1000}$$

$$\mathrm{ESI}\ (\mathrm{min}) = \frac{A_0}{A_0 - A_{10}} \times \Delta t$$

Where A_0 is the absorbance of the diluted emulsion right after it has been homogenized, DF is the dilution factor, C is the protein concentration, φ is the optical path (0.01 m), θ is the oil volume fraction (0.25), and A_{10} is the absorbance after 10 min, $\Delta t = 10$ min

2.11. Determination of rheological properties

According to Li et al. (2021), the samples were measured using rheometers (AR G2 Rheometer, TA Instruments, Crawley, UK) with parallel plate geometry (diameter of 60 mm, a gap of 1 mm). A steady state flow test was conducted to determine the viscosity of samples at different shear rates ranging from 1 to 100 s^{-1}. During an oscillation frequency sweep, the modulus of storage (G′) and loss (G″) were determined at frequencies ranging from 0.1 to 10 Hz with 1 % constant strain. The constant strain was found to be within the linear viscoelastic region. All analyzed samples were conducted at a controlled temperature of 20 °C.

2.12. Statistical analysis and spectral data

All measurements were performed three times. The means of triple measurements were used to represent experiments. The statistical analysis was performed using GraphPad Prism 9 to evaluate the differences among various samples by one-way analysis of variance followed by Dunncan post hoc test (ANOVA, $p < 0.05$). Additionally, principal component analysis (PCA) was applied to the FTIR results to determine the effects of the heating procedure and two pHs on changes in the proteins' secondary structure of the RLPI samples. PCA provided information by creating principal components (PCs) as a coordinated axis with the least amount of information loss possible. Score plots were used to show how the various samples were grouped, and loading plots were used to identify the wavenumbers in charge of classifying the peaks. This analysis was carried out at 95 % confidence interval (Daniloski, McCarthy, O'Callaghan, et al., 2022).

3. Results and discussion

3.1. Visual appearance and thioflavin T fluorescence of RLPI by heated different time

In Fig. 1A, the visual appearance of the RLPI samples during the thermal treatment was presented. As the heating time increased, the color became progressively darker at pH 2, indirectly suggesting the formation of fibers. Fan et al. (2021) previously reported that thermal treatment of whey proteins resulted in the formation of protein aggregates, which coincided with the observed color change, similar to the

Table 1
The average particle size, polydispersity index (PdI), and peak area distribution of RLPI at pH 2.

Samples	Z-Average d.nm	PdI	Pk 1 Mean Int d.nm	Pk 2 Mean Int d.nm	Pk 3 Mean Int d.nm	Pk 1 Area Int Percent	Pk 2 Area Int Percent	Pk 3 Area Int Percent
pH2–0 h	169.3	0.38	178.2	0	0	100	0	0
pH2–1 h	147.6	0.32	132.1	35.92	0	73.4	26.6	0
pH2–2 h	117.4	0.31	167.6	48.05	0	64.9	35.1	0
pH2–4 h	116.1	0.35	152.7	48.01	0	69.1	30.9	0
pH2–6 h	111.9	0.49	186.9	53.72	5437	68.8	29.8	1.4
pH2–12 h	154.9	0.39	252.0	69.11	5477	67.4	31.3	1.3
pH2–18 h	200.5	0.55	433.4	87.74	5026	73.0	24.4	2.5
pH2–24 h	287.9	0.61	403.8	81.78	5560	77.0	21.6	1.4

Table 2
The average particle size, polydispersity index (PdI), and peak area distribution of RLPI at pH 7.

Samples	Z-Average d.nm	PdI	Pk 1 Mean Int d.nm	Pk 2 Mean Int d.nm	Pk 3 Mean Int d.nm	Pk 1 Area Int Percent	Pk 2 Area Int Percent	Pk 3 Area Int Percent
pH7–0 h	80.3	0.34	86.13	5426	0	98.2	1.8	0
pH7–1 h	253.2	0.18	311.8	0	0	100	0	0
pH7–2 h	278.0	0.20	354.7	0	0	100	0	0
pH7–4 h	310.4	0.24	417.6	0	0	100	0	0
pH7–6 h	319.0	0.22	420.0	0	0	100	0	0
pH7–12 h	368.0	0.27	542.9	115.4	0	90.6	9.4	0
pH7–18 h	433.0	0.33	634.9	97.2	0	93.3	6.7	0
pH7–24 h	504.5	0.39	639.9	100.9	0	92.2	7.8	0

Table 3
Total percentage areas of different secondary structures in Amide I of RLPI at pH 2.

Band Assessment	Band frequency (cm^{-1})	Peak area (%)							
		pH2–0 h	pH2–1 h	pH2–2 h	pH2–4 h	pH2–6 h	pH2–12 h	pH2–18 h	pH2–24 h
Side chain	1600–1614	0.59 ± 0.34^{c}	0.50 ± 0.11^{c}	0.71 ± 0.2^{c}	0.43 ± 0.16^{c}	2.18 ± 0.15^{b}	2.85 ± 0.9^{ab}	2.59 ± 0.07^{ab}	3.10 ± 0.4^{a}
Intramolecular β-sheet	1615–1637	50.39 ± 0.19^{a}	47.33 ± 1.36^{b}	49.06 ± 0.14^{ab}	49.58 ± 0.44^{ab}	13.11 ± 0.28^{d}	10.47 ± 2.61^{e}	10.30 ± 0.98^{e}	17.26 ± 0.4^{c}
Random coil	1638–1645	8.30 ± 0.19^{d}	10.90 ± 1.55^{d}	9.32 ± 0.45^{d}	8.38 ± 1.35^{d}	68.62 ± 1.94^{a}	62.72 ± 7.71^{b}	61.48 ± 1.09^{b}	52.79 ± 1.38^{c}
α-helix	1646–1664	36.33 ± 4.61^{a}	39.82 ± 0^{a}	39 ± 0.04^{a}	39.27 ± 1.41^{a}	6.29 ± 1.76^{c}	8.33 ± 1.79^{c}	13.75 ± 0.12^{b}	15.98 ± 1.88^{b}
β-turn	1665–1681	2.36 ± 3.18^{b}	0.24 ± 0.2^{b}	0.56 ± 0.56^{b}	0.59 ± 0.04^{b}	8.12 ± 0.21^{a}	12.10 ± 5.38^{a}	0.79 ± 0.04^{b}	1.75 ± 0.14^{b}
Aggregated β-sheet	1681–1700	2.03 ± 1.09^{cd}	1.20 ± 0.12^{d}	1.36 ± 0.26^{d}	1.74 ± 0.14^{d}	1.69 ± 0.05^{d}	3.54 ± 2.25^{c}	11.08 ± 0.12^{a}	9.12 ± 0.38^{b}

Mean values within a row that do not share a common superscript letter are significantly different ($p < 0.05$)

Table 4
Total percentage areas of different secondary structures in Amide I of RLPI at pH 7.

Band Assessment	Band frequency (cm^{-1})	Peak area (%)							
		pH7–0 h	pH7–1 h	pH7–2 h	pH7–4 h	pH7–6 h	pH7–12 h	pH7–18 h	pH7–24 h
Side chain	1600–1614	2.26 ± 0.13^{de}	1.96 ± 0.29^{cd}	1.31 ± 0.17^{b}	3.12 ± 0.29^{f}	0.36 ± 0.07^{a}	1.60 ± 0.03^{bc}	1.98 ± 0.38^{cd}	2.42 ± 0.13^{e}
Intramolecular β-sheet	1615–1637	66.42 ± 1.64^{d}	9.57 ± 0.26^{a}	10.06 ± 0.6^{a}	13.94 ± 1.69^{b}	47.24 ± 2.75^{c}	8.64 ± 0.39^{a}	8.60 ± 1.22^{a}	9.31 ± 0.12^{a}
Random coil	1638–1645	17.30 ± 0.64^{a}	48.79 ± 0.25^{b}	47.33 ± 0.23^{b}	47.22 ± 3.05^{b}	18.85 ± 5.35^{a}	47.76 ± 2.11^{b}	46.29 ± 0.45^{b}	59.33 ± 6.53^{c}
α-helix	1646–1664	2.28 ± 1.82^{a}	22.87 ± 0.53^{c}	21.68 ± 0.98^{c}	17.60 ± 1.22^{bc}	25.42 ± 8.53^{c}	20.63 ± 0.93^{c}	20.72 ± 1.69^{c}	12.91 ± 6.07^{b}
β-turn	1665–1681	5.17 ± 0.85^{a}	15.54 ± 0.38^{de}	14.42 ± 0.78^{d}	11.91 ± 1.09^{c}	6.67 ± 0.24^{b}	16.05 ± 1.78^{e}	16.81 ± 0.08^{e}	10.59 ± 0.31^{c}
Aggregated β-sheet	1681–1700	6.57 ± 0.61^{c}	1.26 ± 0.14^{a}	5.20 ± 0.35^{b}	6.21 ± 0.18^{c}	1.47 ± 0.15^{a}	5.33 ± 0.18^{b}	5.58 ± 0.05^{b}	5.44 ± 0.18^{b}

Mean values within a row that do not share a common superscript letter are significantly different ($p < 0.05$)

findings of this study. The color became milky at pH 7 with increasing heating time. We speculated that it is due to the formation of particulate protein aggregates or protein denaturation. Phuhongsung et al. (2020) reported that stimulation at different pH altered color, texture, and flavor of soy protein isolate.

The ThT is an amyloid-specific fluorescent dye that can specifically bind to the β-sheet of amyloid fibers and its intensity is generally proportional to the length and concentration of fibril (Arad et al., 2020; Biancalana & Koide, 2010). Fig. 1B depicted the variations in fluorescence intensity with heating process (0–24 h) of RLPI at pH 2 and 7. Lentil proteins that were not heated showed the lowest fluorescence intensity at both pH levels. At pH 2, the ThT fluorescence intensity of RLPI increased dramatically during the brief heating period (1 h), indicating the formation of amyloid fibers. The fluorescence intensity gradually reduced after 6 h of heating. Other research has also discovered a similar trend (Li et al., 2021), which observed that the intensity of fibrils deriving from lentil declined at heating time of above 1 h at pH 2. This phenomenon may be caused by excessive hydrolysis that disrupt the order of nanofibrils (Munialo et al., 2014) or the formation of local gelation (Loveday et al., 2012). At pH 7, the intensity increased rapidly and reached its maximum value after 1 h of heating but remained low throughout the entire heating process. The thermal treatment altered the intramolecular β-sheet content and the fluorescence intensity at pH 2, which was already greater than at pH 7 without heating. It has been reported that the formation of β-sheets was inhibited at higher pH levels due to the damage of hydrogen bonds (Wan & Guo, 2019), that is comparable to the present study's results.

3.2. Transmission electron microscopy (TEM) analysis

The morphologies of RLPI fibrils and particles during the heating process (0 h, 6 h, and 24 h) are shown in Fig. 1C. In order to depict the subtle change of the fibrils, instead of using continuous phase grid (Wynnychuk et al., 2021), in the present study the samples were

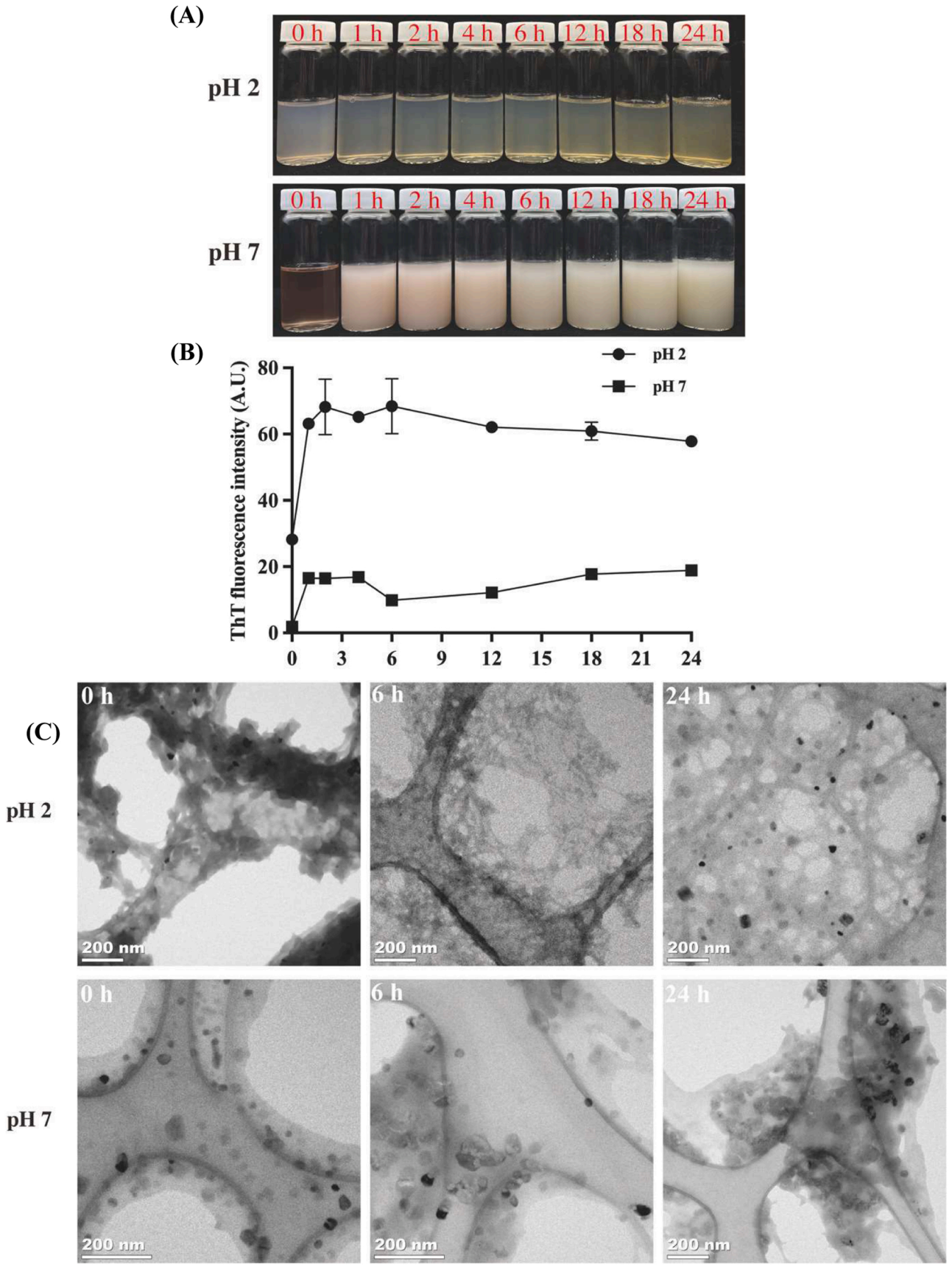


Fig. 1. The visual appearance of RLPI at pH 2 and 7 after heat treatment (A). ThT fluorescence intensity as a function of time for pH 2 and 7 incubated at 85 ℃ (B). Data are shown in mean ± standard error. Transmission electron micrographs (TEM) image of RLPI during the different heated time, the bars within the figures indicate the length of 200 nm (C).

observed by TEM grid since it contains more open spaces and a finer grid structure. Hence, it can better depict the sample's actual situation. Some proteins were linked to the grid at pH 2 before heating. After 6 h of heating, the fibrils were formed, indicating that RLPI experienced self-assembled fibrosis (van der Linden, et al., 2007). It can be seen that a part of the fibrils was connected to the grid through the protein membrane. Kim et al. (2002) reported that thermal treatments of proteins promoted formation of intra- and intermolecular cross-links which might affect the protein film properties, such as gelatin and fibrin protein films. The degree of hydrolysis had an impact on the functional properties of the protein, as extensive hydrolysis resulted in a loss of protein structure and impaired protein film formation (Wouters et al., 2016). In this regard, further heating led to rise of the fibrils' density and appearance of more nodes, thus indicating a formation of fibrillar aggregates. A similar trend was observed when the whey protein isolate solution was incubated under hydrothermal at 110 ℃ and pH 2 at different times (Yang, et al., 2022).

In the current study, the membrane hung on the grid which encases particle protein, as the heating time increased at pH 7, the particle aggregates formed and became greater. Previous research showed that the particulate aggregates formed by hydrophobic and other interactions between globulin proteins at pH 7 were due to random aggregation of the proteins (Jo et al., 2020). Thus, the various particle morphologies revealed that the pH environment would affect the initial shape of the protein, and thermal treatment will not only change its morphology, but also its size, depending on the treatment time as well.

3.3. Sodium dodecyl-sulfate polyacrylamide gel electrophoresis (SDS-PAGE)

The SDS-PAGE results of RLPI over a period of 24 h are presented in Fig. 2. The major bands ranging from 12 to 85 kDa, are depicting the presence of convicilin (62 kDa), 7 S vicilin (50 kDa), 11 S acidic subunits and basic subunits, and also γ-vicilin subunits (Garcia-Mora et al., 2014; Lee et al., 2021). As previously reported, the RLPI samples were acid hydrolyzed and thermally hydrolyzed to produce peptides with decreased molecular weight as heating time increased (Li et al., 2021). At pH 2 (Fig. 2A), the 7 S vicilin protein band was degraded when the heating time was above 4 h. After 12 h, the main protein bands were γ-vicilin subunits and some peptides less than 10 kDa (Tang et al., 2010). Notably, there was protein aggregation in the loading wells observed, which likely indicated the formation of fibrillar aggregates. At pH 7 (Fig. 2B), only thermal hydrolysis was used on the samples. The 7 S vicilin protein band was degraded sharply at 1 h. High-molecular-weight protein bands gradually degraded with thermal hydrolysis ($p < 0.05$). The acidic subunits (around 30 kDa) of the legume protein fraction in RLPI, on the other hand, was not entirely degraded after 24 h.

As described previously, the protein aggregation, particularly vicilin protein was more susceptible to degradation when heated at pH 2 than at pH 7. The lower molecular weight peptides obtained by hydrolysis can assemble into oligomers, which can reassemble into ordered fibrous structures (Wang, et al., 2020). Combining the results of TEM, the

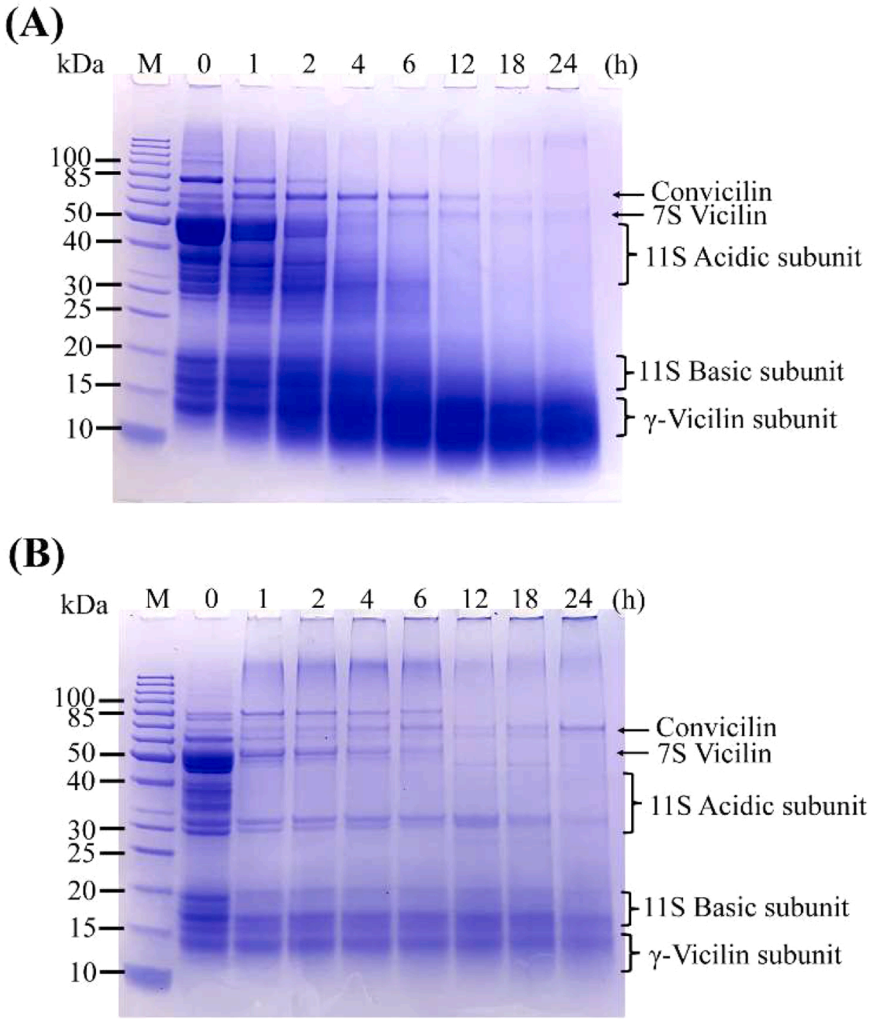


Fig. 2. SDS-PAGE of RLPI samples at pH 2 (A) and 7 (B) for the different heated time (0–24 h). The protein molecular weight (kDa) marker is represented in lane M.

samples were heated for a long time to form aggregated proteins of different shapes.

3.4. Zeta potential and average particle size

The RLPI data for zeta potential and average particle size are presented in Fig. 3 and Fig. S2. The zeta potential measurement investigated the charge intensity on the surface of RLPI, thus according to previous reports, the isoelectric point of RLPI was 4.5 (Alonso-Miravalles et al., 2019). At pH 2 (Fig. 3A), all samples had positive zeta potential values. There was the lowest point (22.13 ± 1.27 mV) when the heated time reached 4 h, then increased to 27.67 ± 1.15 mV over time. Presumably, when the proteins unfold after hydrolysis, charged amino acid groups were exposed on the surface, resulting in an increase of the protein's positive charge (Wynnychuk et al., 2021). In contrast, at pH 7 (Fig. 3B), they all displayed negative zeta potential values (−23.8 ± 0.50 to −25.57 ± 1.07 mV).

The particle size distribution of RLPI was examined at various periods at pH 2 and 7. At pH 2, within 6 h of heating, due to acid hydrolysis and thermal hydrolysis of the protein, the average particle size of the sample gradually decreased (Fig. S2A), as meanwhile, the protein particle size less than 50 nm appeared (Table 1). It was because the protein was degraded into smaller protein fragments by acid hydrolysis, which was consistent with the SDS-PAGE results (Fig. 2). When the heating time increased, there was a slight shifting of the proteins into greater particle size than 5000 nm, accounting for 1.3–2.5 % of the total system. A previous study suggests that any peak at 1000–6000 nm indicates the formation of large protein aggregates (Yang et al., 2018), as in the present study since it was observed that fibrillar aggregation occurred at 6 h. Moreover, the average particle size of legume proteins was shown to decrease during the early heating phase and rose as the heating time increased (Li et al., 2021). At pH 7, the minimum value for unheated protein average particle size was 80.3 nm (Table 2). The average particle size gradually increased within 6 h of heating, and no other size families appeared. As the heating time increased, the smaller particle size families occurred, around 100 nm, accounting for under 10 % of the total system. The increase in PdI suggested that the polydispersity of the sample was growing while its uniformity was decreasing. The lentil protein heated at pH 7 produced particulate aggregates (Wynnychuk et al., 2021). Based on the results of the particle size at various pH levels, it was possible to assume that acid hydrolysis was the primary factor influencing the change in the characteristics of lentil protein isolate and that it was easier to form larger fibrillar aggregates at pH 2 ($p < 0.05$).

3.5. Intensity fluorescence and surface hydrophobicity (H_0) analysis

The change in tertiary structure was monitored using intensity fluorescence. The fluorescence spectrum was based on the change in tryptophan (Trp) and tyrosine (Tyr) residue concentration when the excitation wavelength was 280 nm (Huang et al., 2017).

Alterations in the RLPIs' tertiary structures during hydrolysis induced by heating at pH 2 and 7 were determined and are presented in Fig. 4A and B, respectively. As can be seen in Fig. 4A, when the samples were hydrolyzed and formed fibrils, the fluorescence intensity decreased ($p < 0.05$). There was a red shift in maximum emission wavelengths between 334 and 342 nm, indicating that the peptide chains were extended. When the protein underwent degradation, peptides and hydrophobic groups were exposed. Then the hydrophobic groups on the surface participated in fibrotic assembly causing a decrease in the sample's H_0 (Hu et al., 2019). When comparing the unheated proteins with the heated ones, the fluorescence intensity decreased rapidly and red-shifted, indicating that the thermal treatment significantly impacted the protein's tertiary structural modification at pH 7 ($p < 0.05$). When combined with Fig. 2B, the 7S-vicilin protein bands were rapidly disrupted after 1 h of thermal treatment, and protein particles appeared simultaneously (Fig. S2A). As the heating time increased, the fluorescence intensity decreased and red-shifted, indicating that the heating time altered the microenvironment of Tyr and Trp in the protein, which lead to a decreased hydrophobicity of the protein (Munialo et al., 2014). In addition, the maximum emission wavelength of the pH 2 unheated sample's λmax = 334 nm, and the pH 7 unheated sample's λmax = 328 nm. This demonstrated that the protein structure folded, and the Trp/Tyr residues were reduced in an acidic environment.

The surface hydrophobicity of the protein plays a significant role in its solubility, physical stability, adsorption behavior, and tendency to aggregate (He et al., 2020). The ANS fluorescent probe was frequently employed to assess the degree of denaturation as well as the hydrophobic surface of proteins because it preferred to bind to hydrophobic sites (Hawe et al., 2008). At pH 2, H_0 was gradually reduced from 1240 to 570 when the heating period reached 24 h ($p < 0.05$, Fig. 4C). It was clear from the decrease in H_0 with prolonged heating time that hydrophobic interactions were responsible for the assembly of ordered fibril structures (Hu, et al., 2020). Li et al. (2021) report that lentil protein had an initial increase of the surface hydrophobicity which subsequently decreased during the fibril formation. This study do not show an initial increase, possibly due to the heating time of the first sample being one hour ($p > 0.05$). After 1 h of heating at pH 7, an initial increase in H_0 was observed, followed by a decreasing fluorescence value as heating time increased (Fig. 4C). Under the environment of pH 7, the conformation of the protein could be denatured, and the hydrophobic domain of the protein would be exposed to form a relatively stable structure, which would be slightly affected even if the aggregates appear.

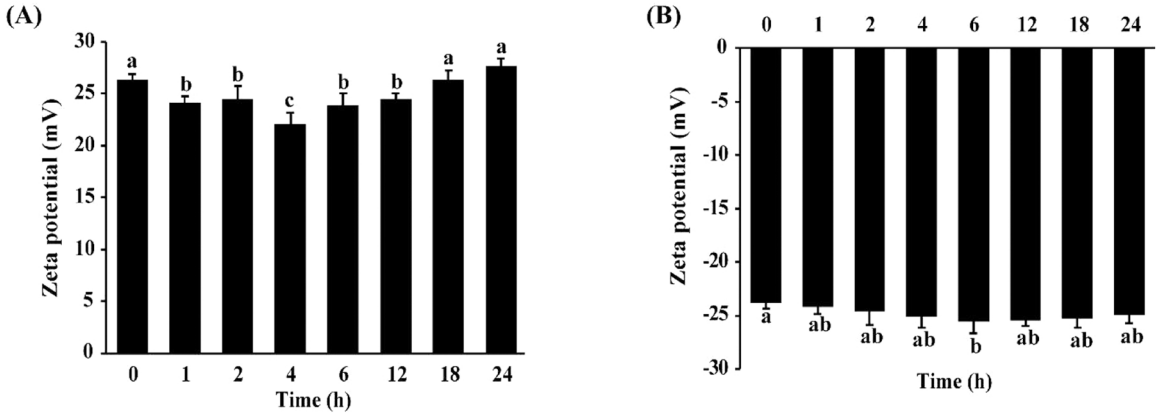


Fig. 3. The zeta potential of RLPI samples at pH 2 (A) and 7 (B) during aggregate formation. Data are shown in mean ± standard error. Different letter represent the significant difference ($p < 0.05$).

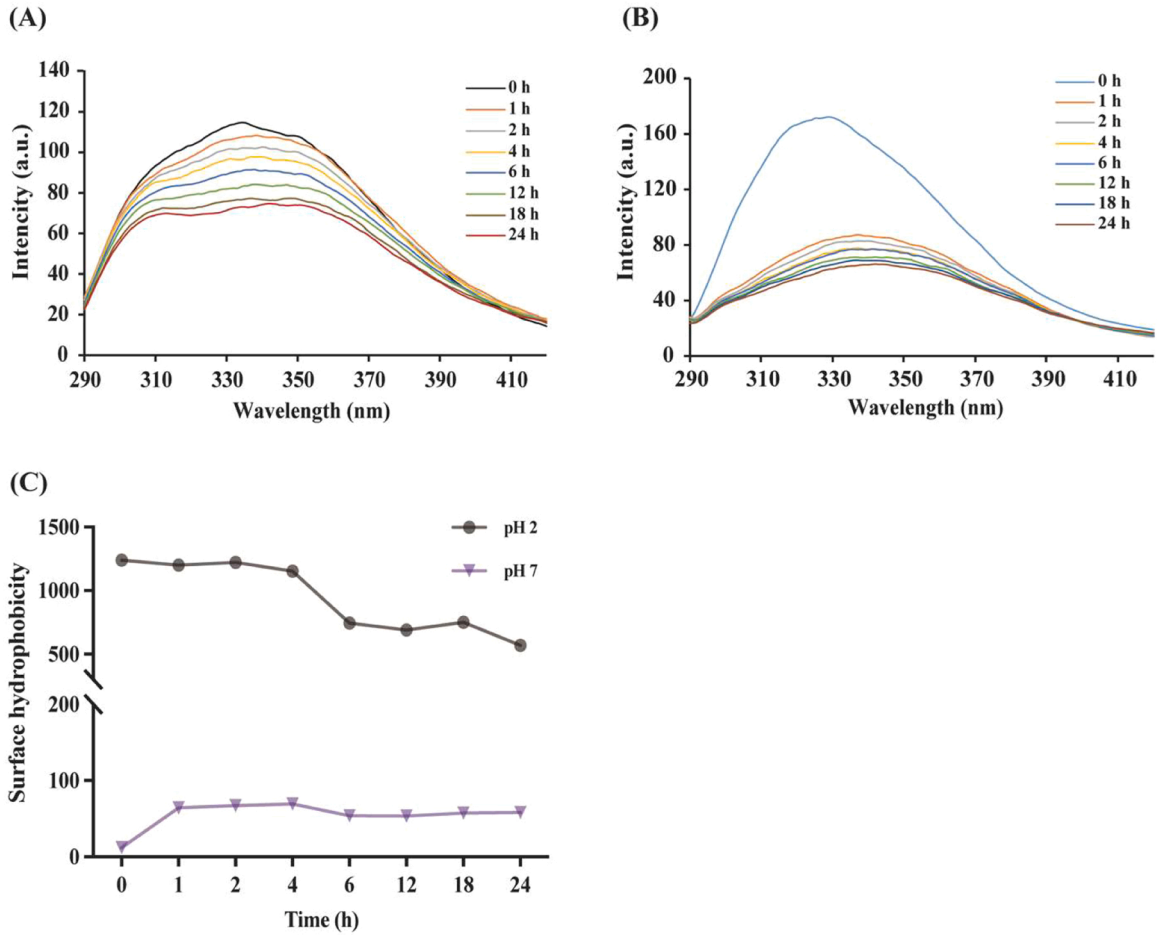


Fig. 4. The Intensity fluorescence of RLPI samples at pH 2 (A) and 7 (B) during aggregate formation. Surface hydrophobicity (C) of RLPI at pH 2 and 7 during aggregate formation.

3.6. Fourier-transform infrared spectroscopy (FTIR)

The deconvoluted FTIR spectra of RLPI aggregates prepared at different pH (pH 2 and 7) were recorded to monitor the conformational changes, and the results are depicted in Fig. S3. The Amide I band area (1700 cm^{-1} - 1600 cm^{-1}) of the polypeptide chain was analyzed using FTIR spectroscopy.

At pH 2, the spectra were changed significantly over the period of 6 h (Fig. S3A1). The intramolecular β-sheet and α-helix in the molecule decreased more sharply during the initial thermal treatment, but the content of the random coil increased rapidly (Table 3). Throughout the prolonged heating, the content of aggregated β-sheet increased. Previous research had shown that the secondary structure of the protein, in comparison to the protein aggregate and the gel of the protein, developed substantial hydrogen bonds between the β-sheet structures, indicating that it may be essential for the formation of 3D networks among fibrillar aggregates (Jo et al., 2020). At pH 7, the content of intramolecular β-sheet decreased rapidly, and α-helix and random coil were increased once heated (Table 4). By comparison of the spectra of unheated samples, the predominant secondary structure of lentil proteins was intramolecular β-sheet. The reason is that the sample was obtained by spray drying. Previous research reported that the content of β-sheet of rice protein isolate obtained by spray drying was higher than that of freeze-dried (Zhao, et al., 2012). The content of α-helix was higher at pH 2 than 7 without thermal treatment. The pH of the environment affected the secondary structure of proteins, which was consistent with results from intrinsic fluorescence. After analyzing the absorption bands, it was observed that the content of intramolecular β-sheet decreased at both pH levels upon heating. This reduction was attributed to the decrease in Trp/Tyr residues resulting from protein unfolding. These findings align with the results obtained from fluorescence intensity measurements (Fig. 4). Namely, Trp/Tyr was favorable for the production of β-sheet, and they participated in the π-π stacking interaction (Hu et al., 2019). Excessive heating, regardless of the pH environment of the protein, will enhance the random coil shape, which may be associated with protein unfolding (Nishinari et al., 2000).

FTIR data is easier to visualize using principal component analysis (PCA) (Grewal et al., 2018). For the pH 2 samples, it can be seen in Fig. S3A2 that the first (PC1, 74.0 %) and second principal components (PC2, 16.2 %) together account for 90.2 % of the variation. The samples heated for more than 6 h were visually separated from others in the score plot along PC1. Furthermore, the samples (0–4 h) were distributed in the positive axe of PC2. The loading principal component (Fig. S3A3) included an intense positive peak at 1624 cm^{-1} referred to as intramolecular β-sheet for PC1, and a negative peak at 1646 cm^{-1} (α-helix) for PC2. For the pH 7 samples (Fig. S3B2), the first (PC1, 70.9 %) and the second principal components (PC2, 18.0 %) accounted for 88.9 % of the variation. The 6 h sample was visually separated from other samples in the score plot along PC1. The loadings on PC1 and PC2 included an intense positive peak at 1624 cm^{-1}, referred to as intramolecular β-sheet, and a negative peak at 1640 cm^{-1} (random coil) for PC1 (Fig. S3B3).

3.7. Emulsifying properties analysis

The emulsifying properties of proteins are commonly evaluated by

the emulsion activity index (EAI) and emulsion stability index (ESI). The maximum surface area formed per gram of protein is shown by EAI, whereas the ability to hold the emulsion structure against changes is shown by ESI (Boye, et al., 2010).

In order for the emulsion to be stable, the protein surface charge is essential. The EAI and ESI of RLPI at different heating times at pH 2 ranged from 38.9 m^2/g (14.3 min) to 51.5 m^2/g, (21.3 min) (Fig. 5A). These results were positively correlated with the zeta potential intensity shown in Fig. 3A, which initially increased and subsequently decreased over time ($p < 0.05$). Previous research had shown that when ovotransferrin was heated at a low pH level, it could form fibrillar aggregates with unique morphologies, and protein fibrils can produce stable Pickering emulsions with enhanced capacities for irreversible interfacial adsorption and anti-aggregation (Wei et al., 2019), as in the current study. It is noteworthy that the EAI decreased by prolonged heating. From the results of EAI, it can be observed that the heating time correlated closely with particle size, implying that the size of excess protein aggregates affects the emulsion properties. Furthermore, gels were generated during the heating of the fiber aggregates. The results showed that proteins heated for 12 and 18 h formed the best stable emulsions ($p < 0.05$). Fig. 5B showed that the EAI and ESI of RLPI at pH 7 ranged from 19.7 to 25.0 m^2/g, and 24.3–35.8 min, respectively. There was no significant difference between the EAI of the treated samples and the untreated sample ($p > 0.05$). Particulate aggregation was formed during the progress of thermal treatment at pH 7. A decrease in the ESI followed by its increase was observed when heated, suggesting that it may be related to protein aggregation and its electrostatic charge. Similarly, in the past it was revealed that surface charge, hydrophobicity, and solubility all affected the EAI and ESI values of protein isolates (Karaca et al., 2011). Compared to pH 7, the EAI of samples at pH 2 was higher, whereas the ESI was the inverse. In comparison to those results, earlier research had shown that low molecular weight surfactants can alter emulsion stability (Mantovani et al., 2018).

3.8. Dynamic rheological properties

The apparent viscosity of RLPI at pH 2 with prolonged heating time was shown in Fig. S4A. It was evident from their shear-thinning behavior that samples were pseudoplastic fluids because their apparent viscosity decreased with increasing the shear rates. The viscosity significantly decreased during the initial- and early- experimental times (1–6 h) and steadily increased with the heating time ($p < 0.05$, 12–24 h). The results were closely related to zeta size (Fig. S2A), with the smallest average size at 6 h and increased at 12 h. As a result of protein denaturation, decreased particle size, and exposing hydrophobic regions, Li et al. (2021) found that cowpea protein's viscosity decreased during the initial phase. During prolonged heating, fibrillar aggregates formed and the viscosity increased. The viscosity of a fluid denoted its resistance to flow and was heavily influenced by molecular interactions. Fibrillar cross-linking by intermolecular contacts may contribute to a denser network, which may herald gel formation (Loveday et al., 2012). The pH, heating time, and concentration of protein affect the formation of lentil protein gels. There was similar shear-thinning behavior at pH 7 (Fig. S4B), but the maximum viscosity of samples occurred at 1 h. When the shear rate reached 100/s, the viscosity of the samples approaches and falls below 0.01 Pa.s, indicating that the intermolecular force is weak (Li et al., 2021).

In the rheological testing, frequency sweeps were performed (Fig. 6). The storage modulus (G') indicates the viscoelastic elastic properties, and the loss modulus (G") represents the viscous properties. Jo et al. (2020) investigated the effect of pH environment, protein concentration and heating time on the formation of gel network structure. The findings revealed that the G" rose with the increasing of the frequency. At pH 2 (Fig. 6A), the samples treated with 24 h heating showed more stable elastic behavior than other samples, and G' was greater than G" in the applied frequency range, indicating that fibrillar aggregates formed a weak gel network structure. As a result of heating for 24 h, ovotransferrin proteins formed protein fibrils that displayed a gel-like behavior as well as an elastic behavior (Wei, et al., 2020). At pH 7 (Fig. 6B), the G' was higher than the G" for all processed samples during initial pried. As the frequency increased, the G' of the samples decreased, which indicated that the samples formed transformed from a weak gel system to a viscoelastic liquid (Barnes et al., 1989). These results corresponded to the viscosity (Fig. S4B). Compared with the above results, G' and G'' at pH 2 were higher than at pH 7 when heated for 24 h, further suggesting that fibrillar aggregates stabilized by hydrogen bonding play a more dominant role in gel strengthening than particulate aggregates (Jo et al., 2020).

4. Conclusion

In this paper the focus has been mainly on the structure-functionality properties of red lentil aggregated protein particles and fibrils, since it is essential to understand the formation progress of the protein aggregates for their successful application in food products. This study first reported the structural changes of proteins during aggregate formation under two pH conditions and explored the relationship between the structural and functional properties of proteins. The formation of fibrillar aggregates, particulate aggregates, and film was observed. How proteins were degraded differs depending on the specific pH, and different shapes of protein and their aggregation developed with prolonged heating. FTIR results showed that, at pH 2 and 7, the intramolecular β-sheet content decreased due to the folding of the proteins by thermal treatment. The emulsifying capabilities of fibrillar proteins were improved than particle proteins. Further, compared to particulate aggregates, fibrous aggregates were more likely to form gel structures through hydrogen bonding.

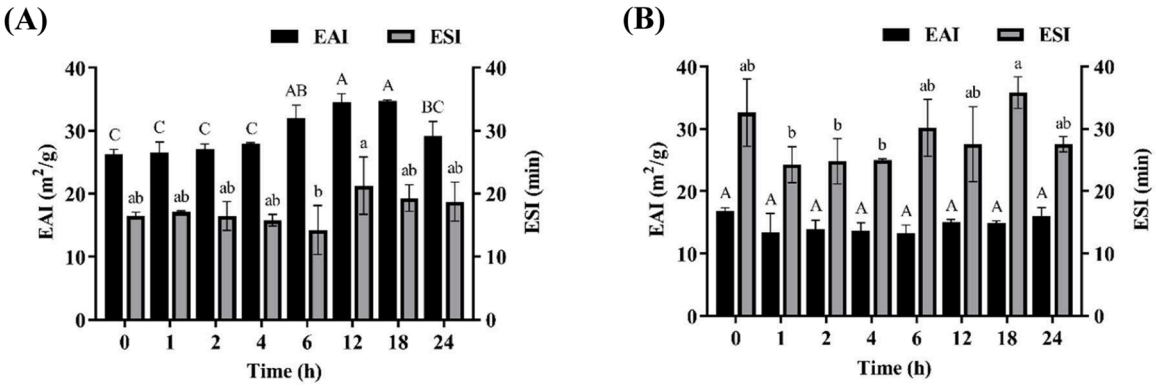


Fig. 5. Emulsifying activity index (EAI) and emulsifying stability index (ESI) of RLPI samples at pH 2 (A) and 7 (B) during aggregate formation. Data are shown in mean ± standard error. Different letter represent the significant difference ($p < 0.05$).

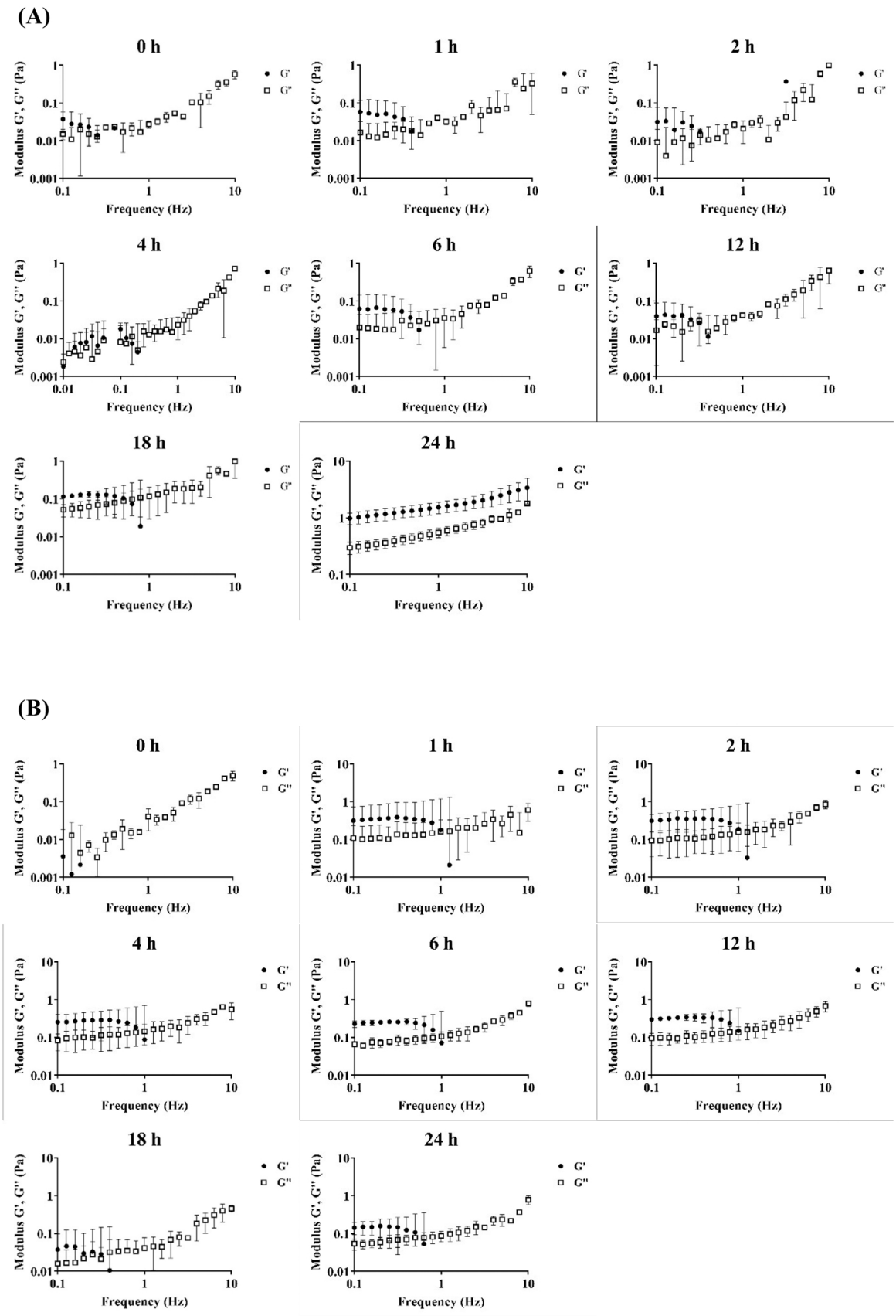


Fig. 6. Frequency dependence of storage modulus (G') and loss modulus (G") at pH 2 (A) and 7 (B) during aggregate formation.

This work is crucial for advancing research on aggregates and fibrils from red lentils and other plant proteins for practical applications. The future research focus should be shifted more towards the application of the red lentil samples, as it has already been the case in the production of microcapsules (Sridhar et al., 2022). However, it's worth noting that ongoing research in the field of plant protein continues to explore their potential and applications.

CRediT authorship contribution statement

Han Du: Conceptualization, Methodology, Data Curation, Writing - Original Draft, Visualization. **Yichen Lin:** Methodology, Review & Editing. **Catherine Stanton:** Writing - Review & Editing, Supervision, Project administration, Funding acquisition. **Davor Daniloski:** Data Curation, Review & Editing. **Emanuele Zannini:** Review & Editing. **R Paul Ross:** Review & Editing. **Song Miao:** Supervision, Conceptualization, Writing - review & editing, Funding acquisition, Project administration, Investigation.

Declaration of Competing Interest

The authors declare that they have no known competing financial interests or personal relationships that could have appeared to influence the work reported in this paper.

Acknowledgments

This work was supported by Teagasc-The Irish Agriculture and Food Development Authority. Han Du was funded under the Teagasc Walsh Fellow Scheme (reference number 2019241). SMATR PROTEIN Project, European Union's Horizon 2020 Research and Innovation Program (No. 862957).

Appendix A. Supporting information

Supplementary data associated with this article can be found in the online version at doi:10.1016/j.foostr.2023.100342.

References

Alonso-Miravalles, L., Jeske, S., Bez, J., Detzel, A., Busch, M., Krueger, M., Wriessnegger, C. L., O'Mahony, J. A., Zannini, E., & Arendt, E. K. (2019). Membrane filtration and isoelectric precipitation technological approaches for the preparation of novel, functional and sustainable protein isolate from lentils. *European Food Research and Technology, 245*(9), 1855–1869. https://doi.org/10.1007/s00217-019-03296-y

Amagliani, L., & Schmitt, C. (2017). Globular plant protein aggregates for stabilization of food foams and emulsions. *Trends in Food Science & Technology, 67*, 248–259. https://doi.org/10.1016/j.tifs.2017.07.013

Arad, E., Green, H., Jelinek, R., & Rapaport, H. (2020). Revisiting thioflavin T (ThT) fluorescence as a marker of protein fibrillation - The prominent role of electrostatic interactions. *Journal of Colloid and Interface Science, 573*, 87–95. https://doi.org/10.1016/j.jcis.2020.03.075

Barbana, C., & Boye, J. I. (2011). Angiotensin I-converting enzyme inhibitory properties of lentil protein hydrolysates: Determination of the kinetics of inhibition. *Food Chemistry, 127*(1), 94–101. https://doi.org/10.1016/j.foodchem.2010.12.093

Barnes, H. A., Hutton, J. F., & Walters, K. (1989). *An Introduction to Rheology* (Vol. 3). Elsevier,.

Biancalana, M., & Koide, S. (2010). Molecular mechanism of Thioflavin-T binding to amyloid fibrils. *Biochimica et Biophysica Acta, 1804*(7), 1405–1412. https://doi.org/10.1016/j.bbapap.2010.04.001

Boye, J. I., Aksay, S., Roufik, S., Ribéreau, S., Mondor, M., Farnworth, E., & Rajamohamed, S. H. (2010). Comparison of the functional properties of pea, chickpea and lentil protein concentrates processed using ultrafiltration and isoelectric precipitation techniques. *Food Research International, 43*(2), 537–546. https://doi.org/10.1016/j.foodres.2009.07.021

Chen, N., Zhao, M., Chassenieux, C., & Nicolai, T. (2016). Thermal aggregation and gelation of soy globulin at neutral pH. *Food Hydrocolloids, 61*, 740–746. https://doi.org/10.1016/j.foodhyd.2016.06.028

Cui, F., McClements, D. J., Liu, X., Liu, F., & Ngai, T. (2022). Development of pH-responsive emulsions stabilized by whey protein fibrils. *Food Hydrocolloids, 122*. https://doi.org/10.1016/j.foodhyd.2021.107067

Curley, D. M., Kumosinski, T. F., Unruh, J. J., & Farrell, H. M., Jr (1998). Changes in the secondary structure of bovine casein by Fourier transform infrared spectroscopy: Effects of calcium and temperature. *Journal of Dairy Science, 81*(12), 3154–3162.

Daniloski, D., McCarthy, N. A., Auldist, M. J., & Vasiljevic, T. (2022). Properties of sodium caseinate as affected by the beta-casein phenotypes. *Journal of Colloid and Interface Science, 626*, 939–950. https://doi.org/10.1016/j.jcis.2022.07.021

Daniloski, D., McCarthy, N. A., O'Callaghan, T. F., & Vasiljevic, T. (2022). Authentication of β-casein milk phenotypes using FTIR spectroscopy. *International Dairy Journal, 129*, Article 105350.

Fan, Y., Peng, G., Pang, X., Wen, Z., & Yi, J. (2021). Physicochemical, emulsifying, and interfacial properties of different whey protein aggregates obtained by thermal treatment. *LWT, 149*, Article 111904.

Garcia-Mora, P., Penas, E., Frias, J., & Martinez-Villaluenga, C. (2014). Savinase, the most suitable enzyme for releasing peptides from lentil (Lens culinaris var. Castellana) protein concentrates with multifunctional properties. *Journal of Agricultural and Food Chemistry, 62*(18), 4166–4174. https://doi.org/10.1021/jf500849u

Grewal, M. K., Huppertz, T., & Vasiljevic, T. (2018). FTIR fingerprinting of structural changes of milk proteins induced by heat treatment, deamidation and dephosphorylation. *Food Hydrocolloids, 80*, 160–167. https://doi.org/10.1016/j.foodhyd.2018.02.010

Gunes, Z. S., & Can Karaca, A. (2021). Examining the amino acid composition, secondary structure, and physicochemical and functional properties of proteins isolated from local lentil landraces of Anatolia. *Cereal Chemistry, 99*(1), 78–89. https://doi.org/10.1002/cche.10446

Hawe, A., Sutter, M., & Jiskoot, W. (2008). Extrinsic fluorescent dyes as tools for protein characterization. *Pharmaceutical Research, 25*(7), 1487–1499.

He, J., Wang, R., Feng, W., Chen, Z., & Wang, T. (2020). Design of novel edible hydrocolloids by structural interplays between wheat gluten proteins and soy protein isolates. *Food Hydrocolloids, 100*. https://doi.org/10.1016/j.foodhyd.2019.105395

Hu, Y., He, C., Jiang, C., Liao, Y., Xiong, H., & Zhao, Q. (2020). Complexation with whey protein fibrils and chitosan: A potential vehicle for curcumin with improved aqueous dispersion stability and enhanced antioxidant activity. *Food Hydrocolloids, 104*. https://doi.org/10.1016/j.foodhyd.2020.105729

Hu, Y., He, C., Woo, M. W., Xiong, H., Hu, J., & Zhao, Q. (2019). Formation of fibrils derived from whey protein isolate: Structural characteristics and protease resistance. *Food & Function, 10*(12), 8106–8115.

Huang, L., Ding, X., Dai, C., & Ma, H. (2017). Changes in the structure and dissociation of soybean protein isolate induced by ultrasound-assisted acid pretreatment. *Food Chemistry, 232*, 727–732. https://doi.org/10.1016/j.foodchem.2017.04.077

Jo, Y. J., Huang, W., & Chen, L. (2020). Fabrication and characterization of lentil protein gels from fibrillar aggregates and the gelling mechanism study. *Food & Function, 11*(11), 10114–10125. https://doi.org/10.1039/d0fo02089c

Joehnke, M. S., Jeske, S., Ispiryan, L., Zannini, E., Arendt, E. K., Bez, J., Sorensen, J. C., & Petersen, I. L. (2021). Nutritional and anti-nutritional properties of lentil (Lens culinaris) protein isolates prepared by pilot-scale processing. *Food Chemistry X, 9*, Article 100112. https://doi.org/10.1016/j.fochx.2020.100112

Karaca, A. C., Low, N., & Nickerson, M. (2011). Emulsifying properties of chickpea, faba bean, lentil and pea proteins produced by isoelectric precipitation and salt extraction. *Food Research International, 44*(9), 2742–2750. https://doi.org/10.1016/j.foodres.2011.06.012

Kim, K. M., Weller, C. L., Hanna, M. A., & Gennadios, A. (2002). Heat curing of soy protein films at selected temperatures and pressures. *LWT - Food Science and Technology, 35*(2), 140–145. https://doi.org/10.1006/fstl.2001.0825

Ladjal-Ettoumi, Y., Boudries, H., Chibane, M., & Romero, A. (2015). Pea, chickpea and lentil protein isolates: Physicochemical characterization and emulsifying properties. *Food Biophysics, 11*(1), 43–51. https://doi.org/10.1007/s11483-015-9411-6

Laemmli, U. K. (1970). Cleavage of structural proteins during the assembly of the head of bacteriophage T4. *Nature, 227*(5259), 680–685.

Lee, H. W., Lu, Y., Zhang, Y., Fu, C., & Huang, D. (2021). Physicochemical and functional properties of red lentil protein isolates from three origins at different pH. *Food Chemistry, 358*, Article 129749. https://doi.org/10.1016/j.foodchem.2021.129749

Li, T., Wang, L., Chen, Z., Sun, D., & Li, Y. (2019). Electron beam irradiation induced aggregation behaviour, structural and functional properties changes of rice proteins and hydrolysates. *Food Hydrocolloids, 97*. https://doi.org/10.1016/j.foodhyd.2019.105192

Li, T., Wang, L., Zhang, X., Geng, H., Xue, W., & Chen, Z. (2021). Assembly behavior, structural characterization and rheological properties of legume proteins based amyloid fibrils. *Food Hydrocolloids, 111*. https://doi.org/10.1016/j.foodhyd.2020.106396

Loveday, S. M., Wang, X. L., Rao, M. A., Anema, S. G., & Singh, H. (2012). β-Lactoglobulin nanofibrils: Effect of temperature on fibril formation kinetics, fibril morphology and the rheological properties of fibril dispersions. *Food Hydrocolloids, 27*(1), 242–249. https://doi.org/10.1016/j.foodhyd.2011.07.001

Mantovani, R. A., de Figueiredo Furtado, G., Netto, F. M., & Cunha, R. L. (2018). Assessing the potential of whey protein fibril as emulsifier. *Journal of Food Engineering, 223*, 99–108. https://doi.org/10.1016/j.jfoodeng.2017.12.006

Mession, J.-L., Chihi, M. L., Sok, N., & Saurel, R. (2015). Effect of globular pea proteins fractionation on their heat-induced aggregation and acid cold-set gelation. *Food Hydrocolloids, 46*, 233–243. https://doi.org/10.1016/j.foodhyd.2014.11.025

Munialo, C. D., Martin, A. H., van der Linden, E., & de Jongh, H. H. (2014). Fibril formation from pea protein and subsequent gel formation. *Journal of Agricultural and Food Chemistry, 62*(11), 2418–2427. https://doi.org/10.1021/jf4055215

Nilsson, M. R. (2004). Techniques to study amyloid fibril formation in vitro. *Methods, 34*(1), 151–160. https://doi.org/10.1016/j.ymeth.2004.03.012

Nishinari, K., Zhang, H., & Ikeda, S. (2000). Hydrocolloid gels of polysaccharides and proteins. *Current Opinion in Colloid & Interface Science, 5*(3–4), 195–201.

Pearce, K. N., & Kinsella, J. E. (1978). Emulsifying properties of proteins: Evaluation of a turbidimetric technique. *Journal of Agricultural and Food Chemistry, 26*(3), 716–723. https://doi.org/10.1021/jf60217a041

Phuhongsung, P., Zhang, M., & Devahastin, S. (2020). Influence of surface pH on color, texture and flavor of 3D printed composite mixture of soy protein isolate, pumpkin, and beetroot. *Food and Bioprocess Technology, 13*(9), 1600–1610. https://doi.org/10.1007/s11947-020-02497-8

Ren, Y., Yuan, T. Z., Chigwedere, C. M., & Ai, Y. (2021). A current review of structure, functional properties, and industrial applications of pulse starches for value-added utilization. *Comprehensive Reviews in Food Science and Food Safety, 20*(3), 3061–3092. https://doi.org/10.1111/1541-4337.12735

Shevkani, K., Singh, N., Kaur, A., & Rana, J. C. (2015). Structural and functional characterization of kidney bean and field pea protein isolates: A comparative study. *Food Hydrocolloids, 43*, 679–689. https://doi.org/10.1016/j.foodhyd.2014.07.024

Sridhar, K., Bouhallab, S., Croguennec, T., Renard, D., & Lechevalier, V. (2022). Application of high-pressure and ultrasound technologies for legume proteins as wall material in microencapsulation: New insights and advances. *Trends in Food Science & Technology, 127*, 49–62. https://doi.org/10.1016/j.tifs.2022.07.006

Tan, M., Zhao, Q., & Zhao, B. (2021). Physicochemical properties, structural characterization and biological activities of polysaccharides from quinoa (Chenopodium quinoa Willd.) seeds. *International Journal of Biological Macromolecules, 193*(Pt B), 1635–1644. https://doi.org/10.1016/j.ijbiomac.2021.10.226

Tang, C. H., Zhang, Y. H., Wen, Q. B., & Huang, Q. (2010). Formation of amyloid fibrils from kidney bean 7S globulin (Phaseolin) at pH 2.0. *Journal of Agricultural and Food Chemistry, 58*(13), 8061–8068. https://doi.org/10.1021/jf101311f

van der Linden, E., & Venema, P. (2007). Self-assembly and aggregation of proteins. *Current Opinion in Colloid & Interface Science, 12*(4–5), 158–165. https://doi.org/10.1016/j.cocis.2007.07.010

Wan, Y., & Guo, S. (2019). The formation and disaggregation of soy protein isolate fibril: Effects of pH. *Food Biophysics, 14*(2), 164–172. https://doi.org/10.1007/s11483-019-09567-1

Wang, Y., Shen, Y., Qi, G., Li, Y., Sun, X. S., Qiu, D., & Li, Y. (2020). Formation and physicochemical properties of amyloid fibrils from soy protein. *International Journal of Biological Macromolecules, 149*, 609–616. https://doi.org/10.1016/j.ijbiomac.2020.01.258

Wei, Z., Cheng, J., & Huang, Q. (2019). Food-grade Pickering emulsions stabilized by ovotransferrin fibrils. *Food Hydrocolloids, 94*, 592–602. https://doi.org/10.1016/j.foodhyd.2019.04.005

Wei, Z., & Huang, Q. (2020). Impact of covalent or non-covalent bound epigallocatechin-3-gallate (EGCG) on assembly, physicochemical characteristics and digestion of ovotransferrin fibrils. *Food Hydrocolloids, 98*. https://doi.org/10.1016/j.foodhyd.2019.105314

Wouters, A. G. B., Rombouts, I., Fierens, E., Brijs, K., & Delcour, J. A. (2016). Relevance of the functional properties of enzymatic plant protein hydrolysates in food systems. *Comprehensive Reviews in Food Science and Food Safety, 15*(4), 786–800. https://doi.org/10.1111/1541-4337.12209

Wynnychuk, C., Jo, Y.-J., Chu, Y., & Chen, L. (2021). Long-term stable emulsions prepared from lentil protein fibrillar aggregates. *Food Structure*, *29*. https://doi.org/10.1016/j.foostr.2021.100204

Yadav, S. S., McNeil, D., & Stevenson, P. C. (2007). *Lentil: An Ancient Crop for Modern Times*. Springer,.

Yang, J., Liu, G., Zeng, H., & Chen, L. (2018). Effects of high pressure homogenization on faba bean protein aggregation in relation to solubility and interfacial properties. *Food Hydrocolloids, 83*, 275–286. https://doi.org/10.1016/j.foodhyd.2018.05.020

Yang, Y., Jiao, Q., Wang, L., Zhang, Y., Jiang, B., Li, D., Feng, Z., & Liu, C. (2022). Preparation and evaluation of a novel high internal phase Pickering emulsion based on whey protein isolate nanofibrils derived by hydrothermal method. *Food Hydrocolloids, 123*. https://doi.org/10.1016/j.foodhyd.2021.107180

Zhang, Y., Liang, S., Zhang, J., Chi, Y., Tian, B., Li, L., Jiang, B., Li, D., Feng, Z., & Liu, C. (2020). Preparation of whey protein isolate nanofibrils by microwave heating and its application as carriers of lipophilic bioactive substances. *LWT, 125*. https://doi.org/10.1016/j.lwt.2020.109213

Zhao, Q., Xiong, H., Selomulya, C., Chen, X. D., Huang, S., Ruan, X., Zhou, Q., & Sun, W. (2012). Effects of spray drying and freeze drying on the properties of protein isolate from rice dreg protein. *Food and Bioprocess Technology, 6*(7), 1759–1769. https://doi.org/10.1007/s11947-012-0844-3